Modeling spatiotemporal carbon emissions for two mega-urban regions in China using urban form and panel data analysis

Meng CAI[1,2], Chao REN[3,4*], Yuan SHI[4,5], Guangzhao CHEN[3,4], Jing XIE[6], Edward NG[2,4]

[1]School of Urban Design, Wuhan University, China

[2] School of Architecture, The Chinese University of Hong Kong, Hong Kong SAR

[3] Faculty of Architecture, The University of Hong Kong, Hong Kong SAR

[4] Institute of Future Cities, The Chinese University of Hong Kong, Hong Kong SAR

[5] Department of Geography & Planning, University of Liverpool, Liverpool, UK

[6] School of Geography and Planning, Sun Yat-Sen University, Guangzhou, China

***Corresponding author**

Email: renchao@hku.hk

Graphical Abstract

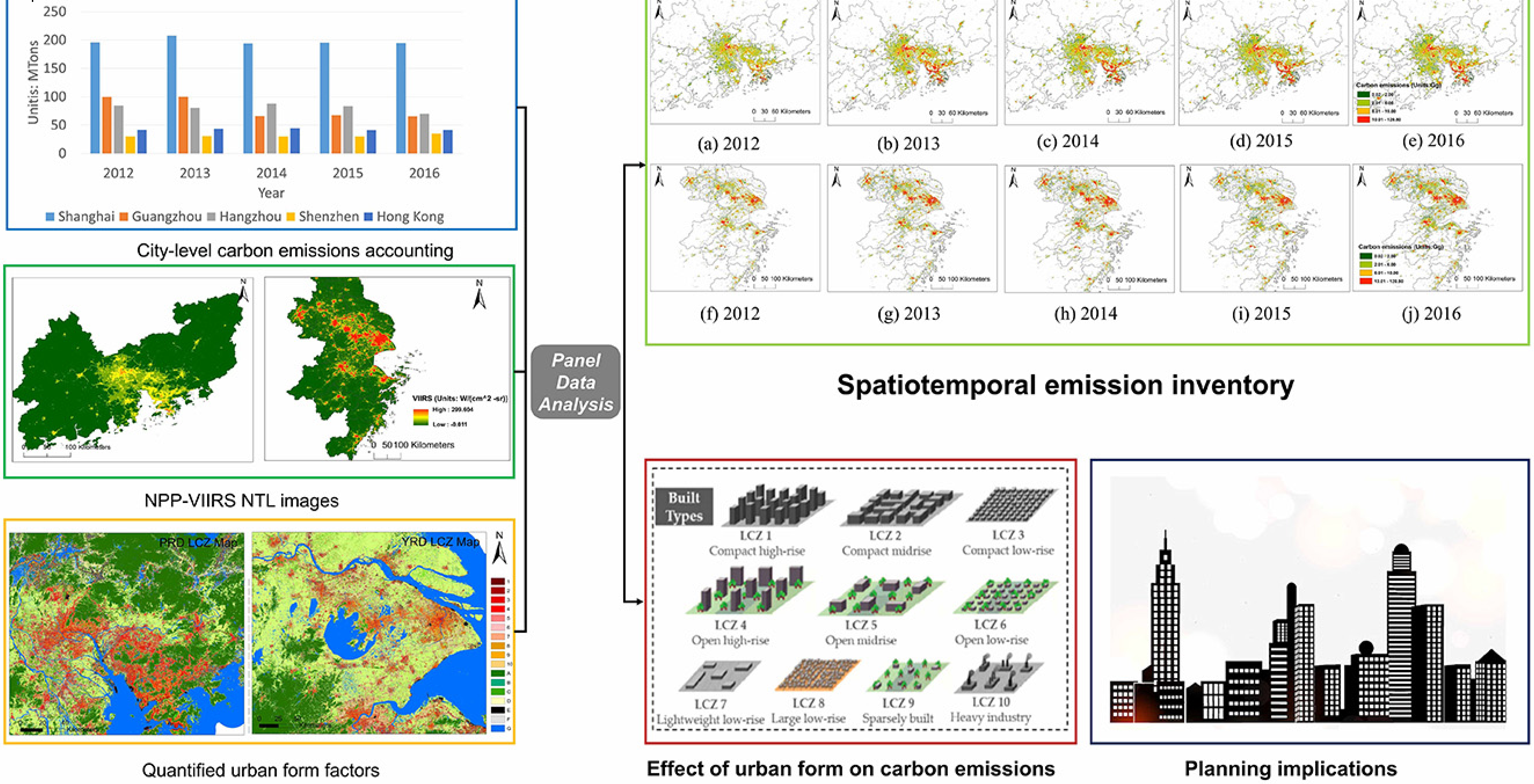

Highlight

- Spatiotemporal (2012-2016) carbon emissions in two mega-urban regions are modeled.
- Urban forms from LCZ maps, NTL images, and a panel data model are used.
- The results show high accuracy (R^2=0.98) and better reveal intra-urban variations.
- Urban compaction and natural landscapes are found to relate to low emissions.
- Scattered low-rise buildings are associated with increased carbon emissions.

Modeling spatiotemporal carbon emissions for two mega-urban regions in China using urban form and panel data analysis

Abstract

Spatiotemporal monitoring of urban CO_2 emissions is crucial for developing strategies and actions to mitigate climate change. However, most spatiotemporal inventories do not adopt urban form data and have a coarse resolution of over 1 km, which limits their implications in intra-city planning. This study aims to model the spatiotemporal carbon emissions of the two largest mega-urban regions in China, the Yangtze River Delta and the Pearl River Delta, using urban form data from the Local Climate Zone scheme and landscape metrics, nighttime light images, and a year-fixed effects model at a fine resolution from 2012 to 2016. The panel data model has an R^2 value of 0.98. This study identifies an overall fall in carbon emissions in both regions since 2012 and a slight elevation of emissions from 2015 to 2016. In addition, urban compaction and integrated natural landscapes are found to be related to low emissions, whereas scattered low-rise buildings are associated with rising carbon emissions. Furthermore, this study more accurately extracts urban areas and can more clearly identify intra-urban variations in carbon emissions than other datasets. The open data supported methodology, regression models, and results can provide accurate and quantifiable evidence at the community level for achieving a carbon-neutral built environment.

Keywords: carbon emission, local climate zone, NPP-VIIRS, panel data, landscape metrics, mega-urban regions

1. Introduction

Climate change has become an important challenge for global sustainable development. As the top carbon producer in the world, China has been deeply involved in global efforts to mitigate climate change. In 2020, China pledged to peak carbon emissions by 2030 and achieve carbon neutrality by 2060 (Xinhua, 2020), which is the first carbon neutrality promise from developing countries. Cities account for more than 70% of total carbon dioxide (CO_2) emissions (IEA, 2021). Hence, they are the principal causes of climate change and the major grounds for achieving carbon neutrality.

Spatiotemporal monitoring of CO_2 emissions in urban areas is crucial for understanding the dynamic patterns and drivers of the carbon cycle and is the foundation for devising strategies and actions to mitigate climate change (Rong, Zhang, Qin, Liu, & Liu, 2020; Jincai Zhao et al., 2019). A reliable fine-resolution CO_2 emission inventory will also be fed into the baseline scenarios for future carbon estimations for carbon peak and neutrality goals. A group of scientists working on climate change issues has further appealed to prioritize high-quality and fine-resolution emission inventories and to understand the interactions between cities and climate for climate change mitigation (Bai et al., 2018). Therefore, it is imperative to conduct an intensive examination of the spatiotemporal heterogeneity of urban CO_2 emissions in China. In particular, the Pearl River Delta (PRD) and the Yangtze River Delta (YRD) are the two largest urban agglomerations in China, with approximately 300 million residents and accounting for about 20% of the country's carbon emissions (Shan et al., 2022). Understanding the carbon emissions of these two mega-urban regions is critical for strategic carbon emission reduction at both national and international scales. Thus, this study focuses on the spatiotemporal CO_2 emissions of the YRD and PRD regions.

In order to assess carbon emissions and facilitate practical mitigation strategies, diverse methodologies have been developed to model spatiotemporal variations in carbon emissions. The bottom-up approach provides the most accurate estimations from emission sources (Gurney et al., 2009; J. Wang et al., 2014). Although securing the most precise estimation from emission sources, bottom-up approaches generally have limited applications in spatiotemporal analysis owing to the lack of detailed data about emission sources, energy consumption, geographical locations, etc. Moreover, inventories from bottom-up methods often have a limited time span and are difficult to perform in multi-temporal analyses.

The top-down method distributes the emissions from a large spatial unit to the required grid based on certain proxy data (Doll, Muller, & Elvidge, 2000). Population and nighttime light (NTL) satellite images are the key proxy data for predicting carbon emissions in top-down models because of their proper representation of human activities, large spatial coverage, and frequent temporal resolution (Doll et al., 2000; Ghosh et al., 2010; Ou, Liu, Li, & Shi, 2015). In particular, NTL data can reflect the socioeconomic situations on the Earth's surface at high spatiotemporal resolution during nighttime (Christopher D Elvidge et al., 1997; Small, Pozzi, & Elvidge, 2005), thereby offering continuous, frequent, consistent monitoring of energy activities and carbon emissions. However, these two datasets have some notable limitations. Population data can reflect human settlement, but they often have a coarse spatial resolution from demographical data and are insufficient to reflect energy activities in non-residential areas. NTL data may underestimate energy activities in non-lit areas such as offices, industries, power plants, and road networks. Therefore, a comprehensive proxy dataset covering various urban structures and land cover types is necessary for a more accurate demonstration of the spatial patterns of carbon emissions.

Urban development and urban forms are the key factors affecting the distributions and magnitude of carbon emissions (C. Li, Song, & Kaza, 2018; Zhilin Liu, Ma, & Chai, 2016; Y. Wang, Hayashi, Chen, & Li, 2014; Xia, Zhang, Sun, & Li, 2017). The effect of urban landscape on the transmission and diffusion of air pollutants can be more profound in high-density urban areas (Yuan, Ng, & Norford, 2014). However, urban forms, specifically urban morphology and land use/land cover information, are rarely used as proxy data for predicting carbon emissions owing to data availability (Cai et al., 2021). Neglecting urban form in modeling carbon emissions may influence the accuracy of the model and lead to an incomplete understanding of the impact of urban form for further planning strategies.

In addition, intra-city planning strategies are substantial for the climate change mitigation action plan (Penazzi, Accorsi, & Manzini, 2019). Cities have proposed their action plan at the city level to facilitate carbon emission mitigation strategies and develop low-carbon cities (Khanna, Fridley, & Hong, 2014). However, the spatial resolution of previous top-down inventories in China was usually greater than 1 km. (B. Cai et al., 2018; M. Li et al., 2017), which is still insufficient to characterize the heterogeneity of carbon emissions within cities and impedes further application in intra-city planning. Inventories with finer spatial resolution are essential for a more precise spatial distribution and more specific actions at the district and community levels.

Moreover, ordinary least squares (OLS) models (Meng, Graus, Worrell, & Huang, 2014; Ou, Liu, Li, & Shi, 2015; Jincai Zhao, Chen, Ji, & Wang, 2018; Juchao Zhao, Zhang, Yang, Zhu, & Ma, 2020) have been frequently used in the top-down method to predict carbon emissions from NTL images. Considering that the relationship between the predictors and carbon emissions can vary over space and time, regular OLS regression models may be biased because of this type of heterogeneity. Adding time or space fixed effects to models can be a highly efficient way to address these invariant characteristics and assess the net effect of the predictors on the response variable. Models with city/province fixed effects have previously been used to estimate CO_2 emissions (Cui et al., 2019; K. Shi et al., 2016;

Zhang, Pan, Zhang, & Xu, 2021). The time-fixed effects that are necessary for controlling the time-specific characteristics of carbon emissions in different years should also be considered in the regression model.

In order to address the limitations of previous studies, the objectives of this study are:

i. To develop a time-fixed effects model to estimate spatiotemporal carbon emissions at a fine resolution using open urban form data
ii. To understand the impact of urban form on carbon emissions of the PRD and YRD regions
iii. To predict carbon emissions of both selected regions during the period 2012 – 2016
iv. To analyze the spatiotemporal variations of carbon emissions of the two regions

2. Material and methods

2.1 Study area

With approximately 20% of China's population and 30% of its gross domestic product (GDP), the PRD and YRD regions are the two fastest growing and leading mega-urban regions in China (Figure 1). The PRD region is located on the southeast coast of China, covering a total area of 56,000 km^2 and consisting of nine megacities in Guangdong Province and two special administrative regions, namely Hong Kong and Macao. As one of the priority economic development zones of China, the PRD region is poised to become the largest bay area in the world with a vital role in facilitating low-carbon and sustainable development (Zhou, Shan, Liu, & Guan, 2018). In July 2010, the National Development and Reform Commission of China released the Notice on the National Pilot Project of Low-Carbon Provinces and Cities, and the PRD region was selected as a pilot area for the national program (National Development and Reform Commission of China, 2010). The Guangdong government also regards green and low-carbon development in the region as a priority to achieve sustainable development and mitigate climate change.

The YRD region comprises the Shanghai municipality, as well as cities in Jiangsu, Zhejiang, and Anhui Provinces. It has become one of the largest megalopolises in the world because of the dramatic and rapid urbanization in this region. In 2019, the resident population of the YRD region exceeded 200 million, accounting for 16.2% of the total population of the country (State Council of China, 2019). In order to meet the huge energy consumption demand in the region, the energy system in the YRD region provides a strong guarantee of rapid economic and social development. A national development strategy, YRD Urban Agglomeration Development Plan was released in 2018 to address the low-carbon development of the region and to enhance the efficiency of urban land use in the region. Thus, to achieve sustainable development of the two mega-urban regions and mitigate global climate change, it is urgent to undertake carbon emission monitoring and spatial optimization strategies to transform the two regions into low-carbon, clean, and efficient urban agglomerations.

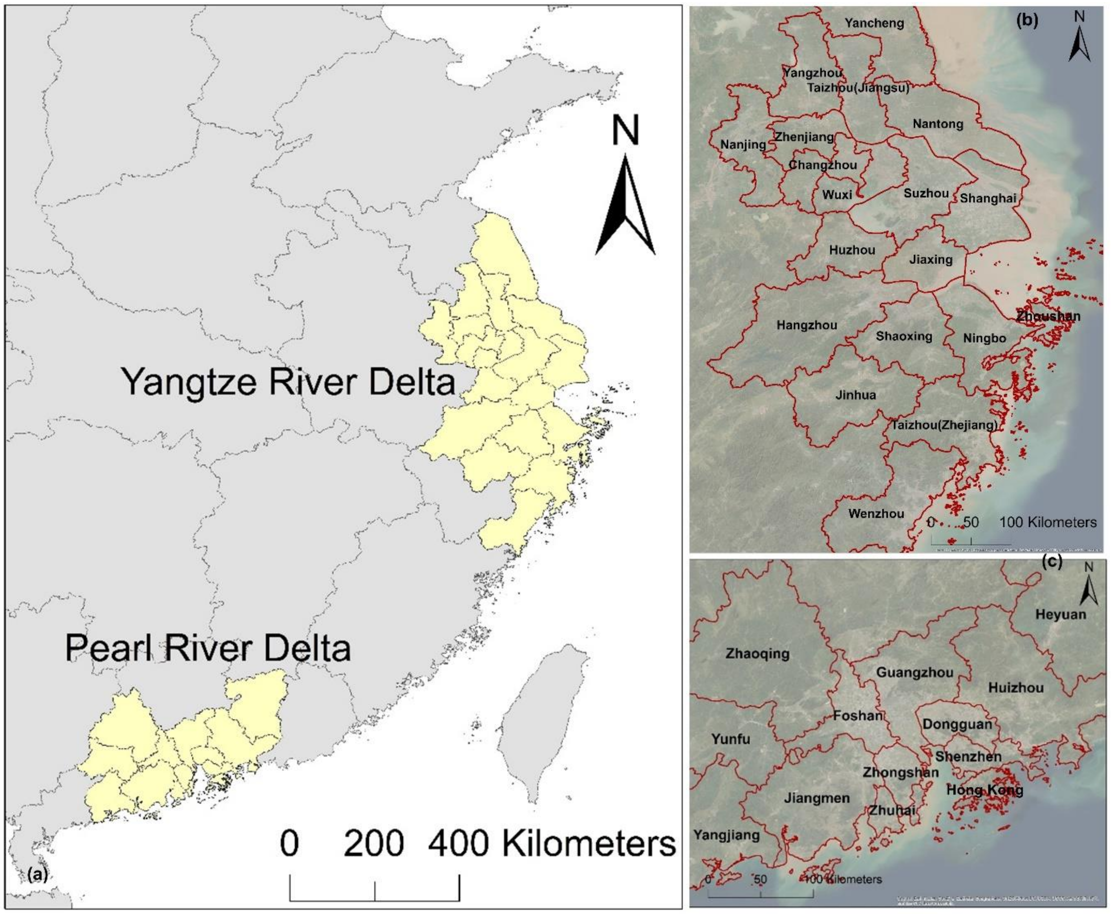

Figure 1 Locations of the study areas (a), cities in the Yangtze River Delta region(b), and cities in the Pearl River Delta region (c)

2.2 Data

2.2.1 Statistical data

Carbon emissions from fossil fuel consumption were calculated for all 30 cities（11 cities in the PRD region and 19 cities in the YRD region）. The latest emission factors were retrieved from Zhu Liu et al. (2015). Data on energy consumption were acquired from the energy balance table of the statistical yearbooks of cities and the country. Socioeconomic information including GDP and population data for each city, was also retrieved from the city statistical yearbooks.

2.2.2 Satellite images

The NPP-VIIRS NTL data has been emerging as a new source of NTL images with a fine spatial grid and free of saturation (Christopher D Elvidge, Baugh, Zhizhin, Hsu, & Ghosh, 2017). It provides the latest nightlight information since 2012 and has a spatial resolution of 500 m × 500 m higher than the DMSP-OLS data (1 km × 1 km). Furthermore, comparative studies demonstrate that the NTL data from the NPP-VIIRS can more accurately represent energy consumption as well as carbon emissions than the DMSP-OLS (Chen, Zhang, Wu, & Cai, 2020; Christopher D. Elvidge, Baugh, Zhizhin, & Hsu, 2013; Ou, Liu, Li, Li, & Li, 2015). Therefore, NPP-VIIRS is more capable of predicting carbon emissions and shows promising predictive results.

This study chose VIIRS Stray Light Corrected Nighttime Day/Night Band Composites as the primary proxy data for predicting spatiotemporal carbon emissions (Mills, Weiss, & Liang, 2013). For each year, the final output of the NTL image was a collection of the mean DN value of the pixels among all monthly products within the year.

As the NPP-VIIRS data have been available since 2012, the study period of this study was from 2012 to 2016 to include the most complete time span of the NTL data and statistical data. Furthermore, as the carbon emissions of megacities in China have been relatively stable since 2012 (Shan et al., 2017), the results from this study period can still provide insight into the current and future carbon emission characteristics of such mega-urban regions.

2.2.3 Local climate zone (LCZ) maps

Urban forms can be characterized by urban morphology and land use/land cover (Ren et al., 2017). The LCZ scheme proposed by Stewart, Oke, and Krayenhoff (2014), provides a standardized way to characterize global cities based on their morphology and function and is therefore suitable for representing urban forms. Compared with previous land use/land cover products with a single urban class, it provides a detailed investigation of the built environments and characterized the land surface structure and cover into 10 built types (LCZ 1-10) and seven natural types (LCZ A-G) (Figure 2).

The scheme has recently gained extensive applications in urban studies because it provides a detailed description of urban structure, uses publicly available data and software, and serves as an internationally recognized standard for the uniform classification of cities across the globe. In particular, the LCZ scheme has demonstrated strong capability in characterizing the spatial distribution of air pollutants (Y. Shi, Ren, Lau, & Ng, 2019). Accounting for urban morphology and land cover through LCZ classification can provide a new opportunity to model the spatial variation of carbon emissions.

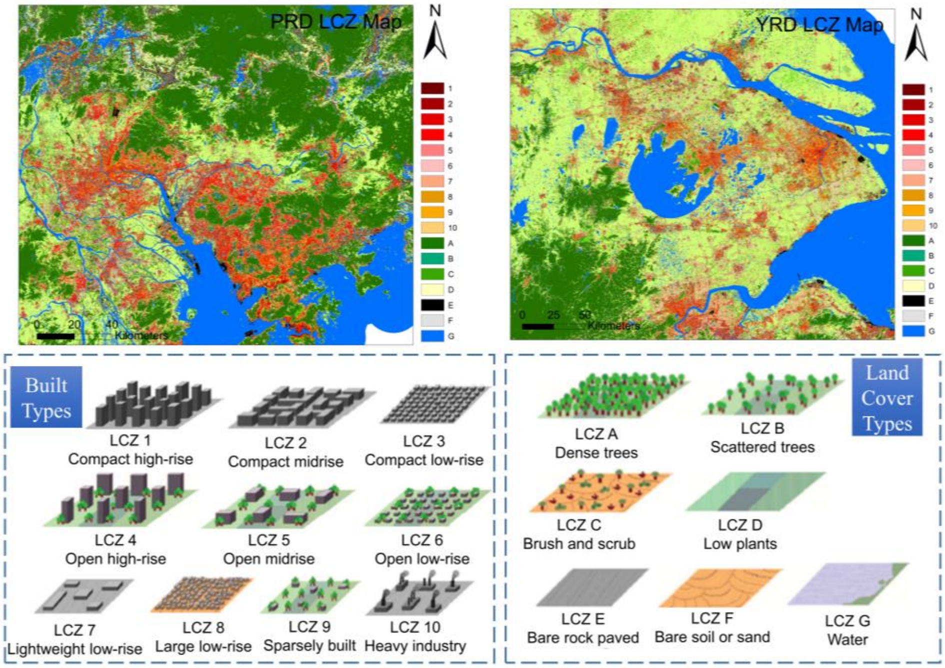

Figure 2 LCZ map of the PRD and YRD regions in 2016

The LCZ maps with 100 m resolution of the two regions from 2012 to 2016 were retrieved from previous studies (Cai, Ren, Xu, Lau, & Wang, 2018; Chung, Xie, & Ren, 2021; R. Wang et al., 2019). They were produced based on various remote sensing products such as Landsat 8, a digital elevation model, Sentinel-1, Sentinel-2, and a random forest classifier. The accuracy assessment showed that their overall accuracy was approximately 73% (M. Cai et al., 2018; Chung et al., 2021; R. Wang et al., 2019).

In order to further link the LCZ maps with land use information for a holistic understanding of the urban structure, this study calculated the percentage of different Essential Urban Land Use (EULUC) developed by Gong et al. (2020) within each LCZ. The EULUC depicts land use information for China in 2018; therefore, we used the LCZ maps in 2016, which is the closest in time to link the land use information.

2.3 Research steps

2.3.1 City-level carbon emissions estimation

Emissions from fossil fuels were calculated based on fossil fuel consumption information and the corresponding emission factors using the IPCC approach (Equation 1)(IPCC, 2006). In this study, the latest emission factors (Zhu Liu et al., 2015) were adopted. Annual fossil fuel consumption data were obtained from the energy balance table of the statistical yearbook of each city.

$$\mathrm{CE_i} = \mathrm{AD_i} \times \mathrm{EF_i} \qquad \text{(Equation 1)}$$

where i represents fossil fuel types summarized by the National Bureau of Statistics of China (2016). AD represents fossil fuel consumption and EF (unit: gCO_2/MJ) is the emission factor that converts the energy consumption to carbon emissions. The city-level carbon emissions can be calculated by aggregating the emissions from all fossil fuel types using (Equation 2).

$$CE = \sum_{i=1}^{n} CE_i \tag{Equation 2}$$

2.3.2 Urban form factors

According to the LCZ maps, the natural LCZ classes (LCZ A-G) were integrated into one class as the natural land cover. To focus on the impact of urban compaction, LCZ 1-6 were reclassified into two categories: compact urban forms (LCZ 1-3), and open urban forms (LCZ 4-6). Therefore, 13 LCZ classes (12 built classes and one natural class) were analyzed in this study.

The urban form of the study area was quantified using a series of metrics that can offer detailed and comprehensive spatial patterns of different land use/landscape types at both class and landscape levels based on LCZ maps (Haines-Young & Chopping, 1996; Neel, McGarigal, & Cushman, 2004). The class-level landscape metrics can describe spatial patterns of classes within a predefined land lot area, including the percentage of landscape types (PLAND), Largest Patch Index (LPI), Aggregation Index (AI) (He, DeZonia, & Mladenoff, 2000), and Connectance Index (CONNECT) (Tischendorf & Fahrig, 2000). Landscape-level metrics can provide information on the diversity of land cover and land use types, including the contagion index (CONTAG) and Shannon's Evenness Index (SEI). The definitions and computation methods of these metrics are summarized in Table 1. There were 52 class-level landscape metrics (13 LCZ classes for each class-level landscape metric) and two landscape-level metrics urban form indicators that were deployed as urban form factors. The 54 metrics were calculated at a 500 m grid level on the Fragstats platform (version 4.2.1) (McGarigal, Cushman, & Ene, 2012).

Table 1 Landscape metrics adopted in this study

Landscape metrics	Definition	Equation*
PLAND	Percentage of the landscape of class i	$PLAND_i = \frac{\sum_{j=1}^{n} a_{ij}}{A}(100)$
LPI	Percentage of the largest patch of the landscape of class i	$LPI_i = \frac{max_{j=1}^{n}(a_{ij})}{A}(100)$
AI	Percentage of like adjacencies to the maximum potential like adjacencies of the corresponding class i	$AI_i = \left[\frac{g_{ii}}{max \rightarrow g_{ii}}\right](100)$
CONNECT	Percentage of functional joins between patches of class i to the total number of potential joins between all Patches of the class	$CONNECT_i = \left[\frac{\sum_{j\neq k}^{n} c_{ijk}}{\frac{n_i(n_i-1)}{2}}\right](100)$

CONTAG	Observed contagion to the maximum potential contagion for the provided classes	$CONTAG = 1 + \left[\frac{\sum_{i=0}^{m} \sum_{q=1}^{m} \left[P_i * \frac{g_{iq}}{\sum_{q=1}^{m} g_{iq}} \right]}{2\, ln\,(m)} * \left[ln \left(P_i * \frac{g_{iq}}{\sum_{q=1}^{m} g_{iq}} \right) \right] \right] (100)$
SHEI	Area composition and richness calculated based on the percentage of each class and the number of classes	$SHEI = \frac{-\sum_{i=1}^{m} (PLAND_i * ln\ PLAND_i)}{ln\ m}$

** i and q are the classes of the landscape; j and k represent the patches in the landscape; m is the total number of classes within the landscape; n is the total number of patches in the landscape; a is the area of the patch; A is the area of the landscape; g refers to the number of adjacencies between pixels of patch types using the double-count method; and c refers to the functional joins (0 = not joined, 1 = joined).*

Furthermore, to focus on carbon emissions in urban areas, this study excluded grids where the natural landscape is completely dominant, that is, grids where the LPI of the natural LCZ is 100%.

2.3.3 Statistical analysis

The NTL data and 54 urban form factors were regarded as potential independent variables whereas the city-level carbon emissions were the dependent variable. Panel data are at the city-year level. The statistical model assumes a linear relationship between the predictors and CO_2 emissions at the city level, and such a relationship can also be applicable at the grid level (500×500 m^2).

In order to eliminate redundancies of the predictors, we performed Least Absolute Shrinkage and Selection Operator (LASSO) regression to determine the optimal subset of predictor variables from all predictors. LASSO variable selection is a supervised algorithm that screens variables that are closely associated with the response variables from a vast number of candidate predictors (Tibshirani, 1996) and is therefore suitable for the relatively large prediction datasets in this study. We further refined the selected variables from the LASSO regression according to the rule of Variance Inflation Factor (VIF)<5 to include only non-collinear variables.

The relationship between city-level carbon emissions and the selected predictors can be established using multiple linear regression (Equation 3):

$$\mathrm{CE_{ij}} = \alpha_1\,\mathrm{V\alpha r_1} + \alpha_2\,\mathrm{V\alpha r_2} + \ldots + \alpha_n\,\mathrm{V\alpha r_n} + \gamma + \varepsilon_{ij} \qquad \text{(Equation 3)}$$

where $\mathrm{CE_{ij}}$ is the city-level carbon emission for city i in year j (2012-2016). α_1..., α_n are the estimated coefficients of the predictors $\mathrm{V\alpha r_1}$ …,$\mathrm{V\alpha r_n}$. γ is the intercept and ε_{ij} is the residual of the model.

Further to the basic model mentioned above, this study considered a linear regression model with time-fixed effects to capture the possible time trends and involve temporal heterogeneity for a more accurate and stable prediction of carbon emissions. The relationship between the predictors and city-level carbon emissions was established, accounting for time-fixed effects (Equation 4):

$$\mathrm{CE_{ij}} = \mathrm{CE_{ij}} = \alpha_1\,\mathrm{V\alpha r_1} + \alpha_2\,\mathrm{V\alpha r_2} + \ldots + \alpha_n\,\mathrm{V\alpha r_n} + \gamma + \boldsymbol{\beta_j} + \varepsilon_{ij} \qquad \text{(Equation 4)}$$

where β denotes the year-specific adjustment to intercept γ in year j. The model was further validated using the F-test and Hausman test to decide between fixed or random effects. Once the relationship was proven by the tests, it was valid to use the selected predictors as proxies to estimate CO_2 emissions via a top-down model. This statistical relationship was then applied to all predictors at the grid level (500 m) for each year to obtain the spatiotemporal carbon emissions.

In addition, the coefficient of each variable was standardized to evaluate the effect of each predictor ((Equation 5).

$$\alpha^{*} = \frac{S_{\mathrm{Var}}}{S_{CE}} \times \alpha \qquad \text{(Equation 5)}$$

where S_{Var} and S_{CE} represent the standard deviations of the predictor and the carbon emissions, respectively, and α is the coefficient of the corresponding predictor in (Equation 4).

Furthermore, the sum of the projected carbon emissions on all grid cells within the administrative boundary of the city can differ from the values in Section 2.3.1. To be consistent with the city-level carbon emissions in the section, we further refined the predicted carbon emissions for each pixel (Equation 6) for each year to adjust the gridded CO_2 emissions (Cui et al., 2019):

$$CE_p = PE_p \times \frac{CE_i}{PE_i} \qquad \text{(Equation 6)}$$

where CE_p is the adjusted carbon emission value for pixel p, PE is the predicted carbon emission based on (Equation 4), CE_i denotes the city-level carbon emission for city i from Section 2.3.1, and PE_i is the sum of predictive carbon emission values within city i.

3. Results

3.1 City-level carbon emissions

Five representative metropolises in the two regions, Shanghai, Guangzhou, Hangzhou, Shenzhen, and Hong Kong, were selected to present their city-level carbon emission (Figure 3). Shanghai, the most populous and economically prosperous city in China, has the highest annual carbon emissions of approximately 200 Mt. The year 2013 was the turning point for carbon emissions in Shanghai, when carbon emissions started to decrease. Guangzhou is the capital and largest city in Guangdong Province. A significant drop in emissions has also been observed in Guangzhou since 2013, with emissions down by half to approximately 60 Mt. The emissions in Hangzhou, the capital city of Zhejiang province, peaked in 2014 during the study period. Shenzhen is the first special economic zone in China and is recognized as one of the fastest-growing megacities in the world. From 2012 to 2015, the total emissions in Shenzhen showed a stable pattern, even under high-speed urban development, which may be attributed to its energy transformation into innovation-based industries. Similar to Shenzhen, the carbon emissions in Hong Kong also showed fewer fluctuations from 2012 to 2016.

Carbon emissions per capita (Figure 3 (b)) are relatively low in Shenzhen and Hong Kong and are below the national average of 7.1 tons (The World Bank, 2020). Shenzhen had the lowest emissions per person, which remained stable during the study period. The per capita carbon emissions of Hong Kong were also relatively low, peaking in 2014. Guangzhou and Hangzhou had the largest emissions per person, at approximately 12 tonnes in 2012 and 2013. The per capita emissions of Guangzhou dropped by 30% in 2014, whereas Hangzhou's per capita emissions began to decline in 2014. The emissions in Shanghai were close to 8 tonnes per person during the study period and began to decrease in 2013.

Shenzhen and Hong Kong account for a large proportion of the modern service and high-tech manufacturing industries. Therefore, these two cities had the smallest carbon emissions per unit of GDP (Figure 3 (c)). Although the total and per capita emissions of Hangzhou did not drop much, the carbon emissions per unit of GDP showed a significant decreasing trend from 2012 to 2016. Shanghai and Guangzhou had the largest amount of carbon emissions per unit of GDP and also witnessed a large decline during the study period, indicating an increase in carbon efficiency with economic growth, as well as the progress of the continuous adjustment and optimization of the energy structure of these cities (Pei et al., 2018).

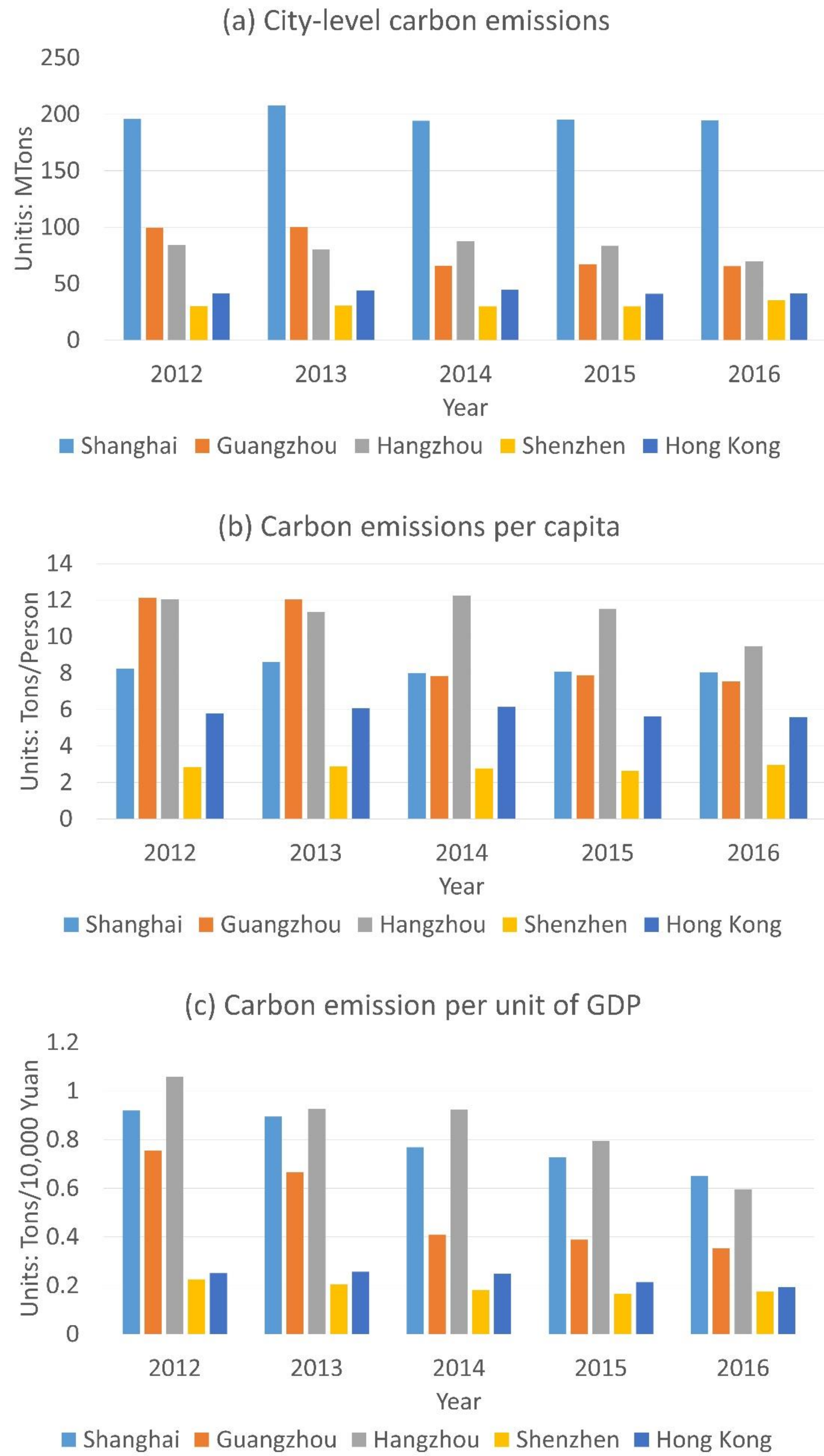
(a) City-level carbon emissions
Unitis: MTons
250
200
150
100
50
0
2012
2013
2014
2015
2016
Year
Shanghai
Guangzhou
Hangzhou
Shenzhen
Hong Kong
(b) Carbon emissions per capita
Units: Tons/Person
14
12
10
8
6
4
2
0
2012
2013
2014
2015
2016
Year
Shanghai
Guangzhou
Hangzhou
Shenzhen
Hong Kong
(c) Carbon emission per unit of GDP
Units: Tons/10,000 Yuan
1.2
1
0.8
0.6
0.4
0.2
0
2012
2013
2014
2015
2016
Year
Shanghai
Guangzhou
Hangzhou
Shenzhen
Hong Kong

Figure 3 City-level carbon emissions of the five metropolises in the two regions; (a) total emissions, (b) emissions per capita, (c) emissions per unit of GDP

3.2 Panel data analysis

Among all potential predictors, 23 with VIF less than 5 remained in the LASSO regression model (see Table S1in Supplementary Material). In particular, NTL data indicated a strong positive correlation with carbon emissions. According to the correlation analysis, NTL alone explained 88.36% (r = 0.94) of the variance in carbon emissions.

The selected predictors were applied in several candidate regression models, including the OLS model, random effect model, year-fixed effects model, and two-way fixed effects model (see Supporting Information). The year-fixed effects model yielded the largest adjusted R^2 (0.98) and F-value, and a significant Hausman Test (p-value < 0.05), thus verifying the applicability of selecting the year-fixed effects model to interpret and predict carbon emissions for the two regions.

Table 2 shows that 11 predictors are statistically significant (p-value < 0.05) in the year-fixed effects panel data model. The percentage of compact urban forms is found to be the most influential with a standardized coefficient of -0.312 and is negatively associated with carbon emissions. Moreover, the LPI of LCZ 7, the aggregation of natural LCZ, LCZ 2, and LCZ 6 demonstrate negative impacts on carbon emissions.

The CONNECT of LCZ 10 showed the largest effect on increasing carbon emissions (standardized coefficient = 0.17). The percentage and LPI of LCZ 9, LPI of LCZ 2 and LCZ 10, and aggregation of LCZ 3 are also inclined to raise carbon emissions.

Table S2 shows the intercepts of the model for each year. It can be observed that 2012 has the largest year-specific constant, indicating that the year has the highest carbon emissions in all cities in both regions over the entire study period. Overall, the carbon emissions in the study area have changed significantly since 2012. The constants continually decreased from 2012 to 2015, and carbon emissions showed a downward trend during this period. The constant for 2016 grew slightly, demonstrating an overall lift of carbon emissions of the cities in the two regions in 2016.

Table 2 Results of the panel data model with year-fixed effects

Predictors	Unstandardized Coefficients	Standardized Coefficients
NTL	$5.03 \times 10^{-4***}$	1.17^{**}
PLAND_Compact LCZ	-3.38^{***}	-0.31^{***}
PLAND_LCZ 9	1.76^{*}	0.07*
LPI_LCZ 9	22.19^{***}	0.08***
LPI_LCZ 10	5.59^{***}	0.12***
LPI_LCZ 2	243.61^{***}	0.13***
LPI_LCZ 7	-103.07^{**}	-0.05**
CONN_LCZ 10	59.00^{***}	0.17***
AI_natural LCZ	-1.09^{*}	-0.13*
AI_LCZ 2	-0.55^{**}	-0.11**
AI_LCZ 3	0.63^{***}	0.12***
AI_LCZ 6	-0.51^{**}	-0.10**
R^2 =0.986	Adjusted R^2 =0.98	
F Statistic	192.39^{***} (df = 28; 77)	

Note: $^{*}p<0.1$; $^{**}p<0.05$; $^{***}p<0.01$

3.3 Spatiotemporal carbon emissions

3.3.1 Overall analysis

The spatiotemporal carbon emissions of the two regions based on the predictive panel data model are shown in Figure 4. In the PRD region, among all years, high emissions (greater than 10 Gg) are generally concentrated in highly urbanized cities, including Hong Kong, Guangzhou, Shenzhen, Foshan, Zhongshan, and Dongguan, owing to the dense urban population and energy activities in these cities. The emissions displayed a more scattered pattern in less-populated cities such as Zhaoqing, Jiangmen, and Zhuhai. High emissions are usually surrounded by medium levels of carbon emissions around the urban fringe, and the emissions gradually decrease from the city cores to rural areas. Moreover, there is no clear boundary for carbon emissions among major cities in the PRD region, demonstrating the formation of a growing urban agglomeration in the region. Larger spatial coverage of high carbon emissions was mostly found from 2013 to 2016 than that in 2012, which may be related to the fact that the total emissions in the region peaked in 2014 (Zhou et al., 2018).

In the YRD region, high emissions were mostly located in the urban cores of Shanghai, Hangzhou, Suzhou, and Wuxi. A notable agglomeration of high emissions was identified among the city group of Suzhou-Wuxi-Changzhou. Other hotspots of high emissions were detected in the urban centers of Nanjing, Ningbo, and Jiaxing. The carbon emission in the southern part of the YRD region presented a highly decentralized distribution pattern, and the concentration of carbon emissions in the northern part was significantly greater than that in the southern part. Low emissions (less than 2 Gg) were most distributed on the fringes of urban centers. The inter-annual spatial variations are relatively insignificant since the growth rate of carbon emissions peaked in 2007 (Tang, Zhang, & Bethel, 2019).

According to the change from 2012 to 2016 (Figure S1), significant increases in carbon emissions were concentrated in the major urban cores in the two regions, whereas the reduction of emissions is in a more decentralized manner. There is an overall increase in the magnitude of carbon emissions in most urban areas of the two regions, which can result from the urban expansion process of the cities during the study period. In the PRD region, the reduction in carbon emissions was scattered in Guangzhou, Foshan, Dongguan, Shenzhen, and Zhongshan. In the YRD region, the decline was primarily identified in the urban areas of Shanghai, Changzhou, Ningbo, and Hangzhou, as well as in the suburbs of Shaoxing and Wenzhou.

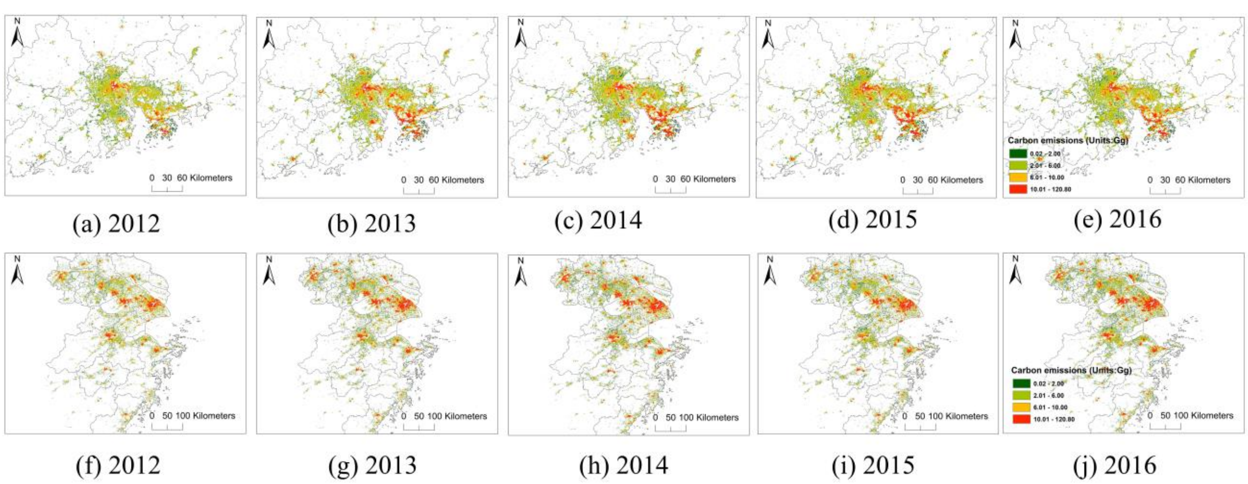

(a) 2012 (b) 2013 (c) 2014 (d) 2015 (e) 2016

(f) 2012 (g) 2013 (h) 2014 (i) 2015 (j) 2016

Figure 4 Spatiotemporal variations of carbon emissions of the PRD region (a-e) and YRD region (f-j)

3.3.2 Year-on-year changes in CO_2 emissions

Figure 5 reveals the yearly changes in gridded CO_2 emissions in the two regions. From 2012 to 2013, the PRD region witnessed significantly increased emissions in most cities, which is likely related to the continuous urban expansion during this period (Figure 5 (a)). Dispersive declines were also observed in Guangzhou and Foshan. Similar to the PRD region, there was a large increase in carbon emissions in the YRD region from 2012 to 2013. Some scattered decreases were observed in Nanjing, Suzhou, and Hangzhou.

Between 2013 and 2014, a large expansion of emission decrease has been detected in the PRD region, covering most of the urban areas of Dongguan, Guangzhou, Foshan, Zhongshan, Zhaoqing, and Yunfu. Some concentrated growth is located in Hong Kong and Shenzhen while some scattered increases are in other cities in the region. Meanwhile, the YRD region is concurrent with a more mixed pattern of growth and decline in carbon emissions (Figure 5 (f)). Frequent blue pixels that represent declines are distributed in the urban cores of the region, especially in Shanghai, Hangzhou, Ningbo, Nanjing, and Suzhou-Wuxi-Changzhou. The increases were more often distributed in the urban fringes of the YRD region.

Between 2014 and 2015, the PRD region experienced a large decline in emissions in most cities, especially Hong Kong, Shenzhen, Guangzhou, Foshan, and Zhongshan (Figure 5(g)). The decline hotspots shifted from the southwest to the southeast of the region compared to the changes from 2013 to 2014. Some scattered increases were identified in Guangzhou, Shenzhen, and Foshan. The YRD region also showed a prevailing decrease in emissions, with some increases in Shanghai and Suzhou (Figure 5(c)). The spatial patterns showed fewer variations in the urban fringes of the two regions during the study period.

Between 2015 and 2016, the PRD region exhibited a generally downward pattern (large area covered with blue and yellow color in Figure 5 (d)), whereas some mixed changes were identified in the Guangzhou-Foshan area. Further declines in carbon emissions have been observed in the major cities in the PRD region, including Guangzhou, Shenzhen, Foshan, and Hong Kong. In contrast to the downward trend in the PRD region, the YRD region has growing carbon emissions in the urban centers of most cities (Figure 5 (h)). Concentrated reductions in carbon emissions were also observed in the urban centers of Shanghai.

In general, yearly changes in carbon emissions in the PRD region are more uniform and show an overall decreasing pattern, demonstrating that the region has achieved integrated and coordinated development. However, the year-on-year changes in the YRD region are more diverse and mixed in different cities, indicating that coordinated development has not yet been fully realized in the region, and the emission reduction measures and effects are not consistent across cities.

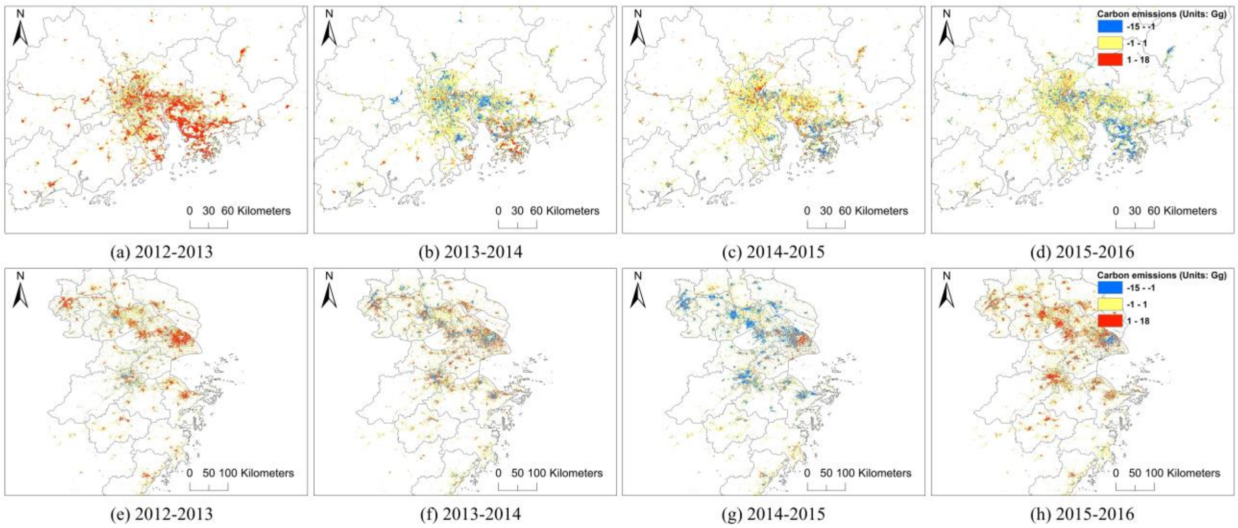

Figure 5 Year-on-year change in carbon emissions from 2012 to 2016 in the PRD region (a-d) and YRD region (e-h)

4. Discussion

4.1 Influential urban form and planning implications

4.1.1 Urban compaction

Low-carbon strategies at both the community and city levels can be devised based on the effects of landscape metrics (Section 3.2) and land use information (Table S3 from LCZ maps). Urban compaction (LCZ1-3) has the minimum standardized coefficient and is, therefore the most influential urban form factor in decreasing carbon emissions. A compact urban layout and planning can reduce travel distance, thus abating transport-related carbon emissions. Moreover, compact development may have more efficient interactions among different zones (Yeh & Li, 2001; Yu, Wu, Zheng, Li, & Tan, 2020) and, therefore, can reduce energy consumption in different sectors. Hence, this study recommends compact and centralized urban development rather than decentralized distribution in the future urbanization processes in the two regions. It is also imperative for urban planners and decision-makers to accommodate sufficient public transportation facilities and improve the accessibility of the road networks of the two regions. Nevertheless, arbitrarily increasing the size of compact urban settlements can increase anthropogenic carbon emissions and should therefore be considered carefully when developing compact settings with various heights and functions.

Accordingly, panel data analysis can provide an in-depth and detailed understanding of the impacts of different compact urban forms on carbon emissions based on the effects of landscape metrics for LCZ 1-3. The landscape metrics of LCZ 1 yield insignificant results in this study. The LPI of LCZ 2 (compact middle-rise buildings) can raise carbon emissions, whereas the aggregation of LCZ 2 is related to low emissions. Compact middle-rise buildings are common and crucial urban forms often with commercial and residential functions in both regions (Table S3). The results of this study offer insights into the design of essential urban forms where compact mid-rise buildings should be clustered together. Meanwhile, the size of the aggregated patch of LCZ 2 should be restricted to avert the dominance of LCZ 2. Compact low-rise buildings (LCZ 3), which are primarily dense commercial areas and urban villages, prefer relatively scattered layouts, based on the panel data model. The concentrated pattern of LCZ 3 is likely related to the high population density and increased energy consumption from commuting and commercial activities.

4.1.2 Other urban forms

The aggregation of LCZ 6 (open low-rise) is also associated with lower emissions. Open low-rise buildings often belong to large commercial or recreational areas with high emissions from both the residential and business sectors (Table S3). This finding provides evidence for the planning of villa areas and resorts that they should be allocated in an aggregated manner to reduce traffic-related emissions and inter-zone energy activities.

The panel data model also indicates that the total area and area of the LPI of LCZ 9 (scattered low-rise buildings) are related to high emissions. LCZ 9 is a typical residential building type in rural areas. Sparse building settings can increase travel distances and lead to increased transport-related emissions. Accordingly, this study suggests restricting the proportion and size of scattered low-rise buildings to avoid making LCZ 9 the dominant urban form of community to achieve low-carbon development.

Heavy industrial areas (LCZ 10) are often associated with high emissions, because factories can generate pollutants during industrial processes. The LPI and CONNECT of LCZ 10 can increase carbon emissions, providing evidence and knowledge for planning industrial areas in the two regions. In the process of energy transformation, the total area of industries does not necessarily induce high emissions in either region; however, it is necessary to control the area of the largest patches of factories and industrial facilities. It is also necessary to reduce the connectivity of industrial areas by increasing the distance between the different patches. Therefore, this study proposes that when heavy industrial areas are the primary land use, they should be distributed in a decentralized manner, with other land uses spaced in between. The results of this study also encourage an increase in the dominance of lightweight buildings (LCZ 7), which are typically manufactured and warehouse buildings located in rural areas (Table S3). When LCZ 7 is the major land use type, it tends to indicate low urbanization rates and building energy consumption.

Furthermore, the AI of the natural landscape (LCZ A-G) is related to lower emissions, which indicates that the natural landscape should have certain aggregation and dominance in land use planning at both the community and city levels.

4.2 Comparison with other datasets

The spatial distributions predicted in this study are compared with the original NPP-VIIRS NTL images and the FFDAS version 2.2 dataset at a 10 km resolution (Asefi- Najafabady et al., 2014) to evaluate the performance of the results. The FFDAS models the spatial distribution of global carbon emissions from DMSP NTL data, population data, and power plant emissions for the period 1997-2012. Hence, 2012 was selected for comparison and the results from this study were further aggregated to the same spatial grid of the FFDAS to ensure consistency between the two datasets. We calculated the difference between the two datasets by pixels (FFDAS minus PRE).

For the identification of urban areas, the results from the present study extract the largest urban areas compared to the NPP-VIIRS data and FFDAS, not only in urban centers but also in suburbs and less-populated areas such as the isolated points in Hangzhou, Nantong, and the southern PRD region. This study adopted LCZ maps generated from multi-source satellite images to extract urban areas, which can identify urban areas with potential energy activities during both day and night according to the spectral characteristics of the earth's surface that are independent of diurnal variation. However, NTL images can only identify lit areas during the nighttime; therefore, it is likely to underestimate urban areas without human activities during the nighttime. Therefore, this study can more accurately and comprehensively extract urban areas than previous datasets that only adopted NTL data as the primary proxy data by exploiting LCZ maps.

Moreover, compared to the original NPP-VIIRS images and the FFDAS dataset, this study more clearly characterizes the intra-urban variations in carbon emissions. The FFDAS has a coarse spatial resolution and is not able to detect intra-urban variations in carbon emissions. The NTL data have relatively uniform magnitudes of carbon emissions in urban centers, whereas the results of this study show larger fluctuations in cities of these two regions. Greater intra-urban variations can be more realistic because the brightness of the light is not necessarily related to the intensity of energy activity, and buildings with similar brightness can have different energy consumption magnitudes; the LCZ maps contain information on urban forms and functions that can assist in reflecting the heterogeneity of energy activities.

The differences between FFDAS and the results of the current study are shown in Figure 6 (d) and (h) by subtracting the results of this study with FFDAS in the same 10 km spatial grid. The green pixels show the locations where the FFDAS has larger values (more than 0.5 standard deviations), whereas the brown color indicates that the value from this study is higher. Overall, the differences between the two for the majority of the pixels are minor (less than 0.5 standard deviations). In the PRD region (Figure 6 (d)), large differences are not frequent, and the results of this study have relatively larger values in the western part of the region, which is relatively unprosperous. The green pixels where the FFDAS is higher, are scattered in this region. For the YRD region (Figure 6 (h)), this study has higher values in the north part of the region, Jiaxing, and Huzhou. The green pixels are primarily located in Shanghai and Suzhou, the two most prosperous cities in this region. In summary, this study demonstrates high values of carbon emissions in relatively less developed cities under rapid urbanization compared to FFDAS data. This mismatch is in accordance with a previous finding that NTL data have relatively poor performance in less developed than in developed regions and can underestimate emissions in these regions (Doll et al., 2000). Therefore, the comparison further highlights the necessity of supplementing urban form information to improve the deficiencies of NTL data in unprosperous areas when modeling carbon emissions.

Overall, the results from this study have the strengths of more proper extraction of urban areas, the ability to characterize intra-urban variations in carbon emissions, and more accurate prediction in less-developed areas.

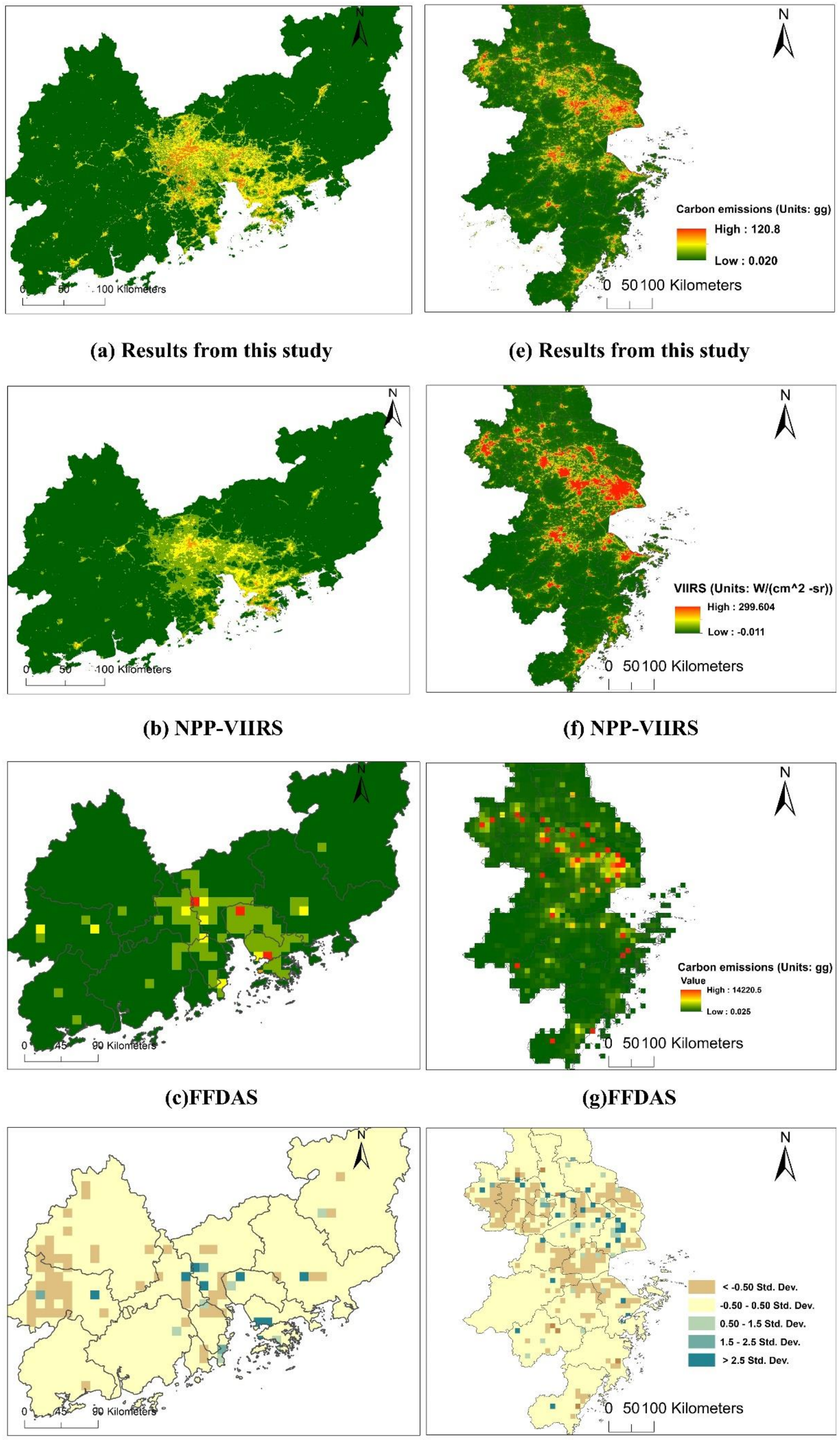

(a) Results from this study **(e) Results from this study**

(b) NPP-VIIRS **(f) NPP-VIIRS**

(c)FFDAS **(g)FFDAS**

(d)FFDAS-PRE **(h) FFDAS-PRE**

Figure 6 Comparison with other data sources, (a-e) for the YRD region, and (f-h) for the PRD region

4.3 Limitations and future work

This study has several limitations. First, the emission factors for each energy activity remain subject to large uncertainties. There are various sources of emission factors, such as the IPCC on Climate Change (IPCC, 2006), and China's National Communication (Development & Commission, 2012). We attempted to minimize this problem using localized coefficients proposed by Zhu Liu et al. (2015). The emission factors were revised according to independently evaluated activity data and two comprehensive measurement datasets in China. There are also uncertainties in proxy data that disaggregate carbon emissions. Although the NPP-VIIRS has the finest spatial resolution among all the instruments onboard the S-NPP satellite, it can have background noise (Christopher D Elvidge et al., 2017) and geolocation errors (W. Wang, Cao, Bai, Blonski, & Schull, 2017). In addition, the LCZ maps have an overall accuracy of 73.2% and have relatively poor performance for classes such as LCZ 9, LCZ B, and LCZ C (M. Cai et al., 2018; Chung et al., 2021; R. Wang et al., 2019). Therefore, we propose combining other high-quality urban form data with the LCZ data to minimize the modeling error.

In the future, we plan to include other open urban data with high spatiotemporal resolution, such as human activity data from social media applications. In addition, the development stages of cities can influence the effects of urban form on carbon emissions. Further studies will use larger data samples to account for the developmental stages in the modeling. Also, the impact of urban development on carbon emissions may not be linear, which is not reflected in the current linear models. We plan to adopt more advanced models, such as neural networks or random forests (Hu et al., 2017; Huang et al., 2018; Xu et al., 2018) that can incorporate nonlinear and complex relationships in the modeling of carbon emissions, to achieve higher accuracy than that of previous models. The spatiotemporal inventories created in this study can serve as a baseline for future carbon emission projections to examine progress towards carbon neutrality. The inventories will be updated annually to support carbon audit and mitigation strategies.

5. Conclusions

This study analyzed the effects of urban forms that were generated from LCZ maps and landscape metrics on carbon emissions in the PRD and YRD regions. Moreover, carbon emissions at 500 m resolution of the two regions from 2012 to 2016 were predicted from NTL data and urban forms using panel data regression.

The following conclusions can be drawn from this study: 1. Both NTL data and urban form factors are found to be significantly associated with carbon emissions of the two regions in the year-specific panel data model (R^2 = 0.98). 2. The panel data model indicates that there is an overall decrease in the carbon emissions of the two regions since 2012 and a slight elevation from 2015 to 2016. 3. Urban compaction and natural landscape are found to relate to low emissions, whereas scattered low-rise buildings are associated with rising carbon emissions. 4. There are notable spatial variations in carbon emissions, although city-level carbon emissions are generally stable for most cities in both regions during the study period. In particular, the YRD region has larger emission hotspot expansions than the PRD region. 5. Compared to the original NTL data and the FFDAS data, the results from this study extracted urban areas more accurately and can more clearly identify the intra-urban variations in carbon emissions.

The results offer several important policy implications for urbanization progress towards carbon neutrality in the two mega-urban regions. First, although a compact urban form is generally beneficial for reducing carbon emissions, it is also necessary to investigate the effects of different building heights and functions in a compact urban environment. Second, compact middle-rise buildings should be clustered on a relatively small scale within the community. Third, compact low-rise buildings favor a more scattered layout. In addition, open low-rise buildings should exhibit aggregated patterns. Furthermore, this study suggests limiting the size, proportion, and dominance of scattered, low-rise buildings. In addition, industrial areas should be distributed in a decentralized manner, and the distance between patches should be increased. In addition, there should be a greater concentration of natural landscaping and predominantly lightweight low-rise buildings.

This study is novel in several aspects. First, this study is the first to incorporate detailed and comprehensive urban form factors from LCZ maps in carbon emission modeling, providing an accurate estimation of the spatial variations in carbon emissions. Second, carbon emissions are modeled using a panel data model with time-fixed effects rather than OLS models, accounting for the temporal dimensions of carbon emissions. Third, the research framework only adopted open data and utilized an internationally accepted scheme of urban form, thereby demonstrating the effectiveness and potential of applying the method to other cities and regions worldwide and identifying opportunities for global efforts to reduce carbon emissions. Therefore, urban planners, architects, and decision-makers can refer to the developed methodology, regression models, and spatiotemporal inventories to jointly foster a carbon-neutral built environment.

Acknowledgment

This study is supported by the CRF project entitled "Turning 2060 Carbon Neutrality into Reality: a cross-disciplinary study of air pollution and health co-benefits of climate change mitigation of the Guangdong-Hong Kong- Macau Greater Bay Area (GBA)" (C7041-21GF). The authors would like to thank the CUHK Sustainable and Environmental Design Group and Prof. Edward Ng for providing a parttime studentship. The authors are also grateful to Miss Zhuo Chen from the Carroll School of Management at Boston College for her valuable advice on the statistical analysis of this study.

Reference

Asefi-Najafabady, S., Rayner, P., Gurney, K., McRobert, A., Song, Y., Coltin, K., . . . Baugh, K. (2014). A multiyear, global gridded fossil fuel CO2 emission data product: Evaluation and analysis of results. *Journal of Geophysical Research: Atmospheres, 119*(17), 10,213-210,231.

Bai, X., Dawson, R. J., Ürge-Vorsatz, D., Delgado, G. C., Barau, A. S., Dhakal, S., . . . Roberts, D. C. (2018). Six research priorities for cities and climate change. In: Nature Publishing Group.

Cai, B., Liang, S., Zhou, J., Wang, J., Cao, L., Qu, S., . . . Yang, Z. (2018). China high resolution emission database (CHRED) with point emission sources, gridded emission data, and supplementary socioeconomic data. *Resources, Conservation and Recycling, 129*, 232-239. doi:10.1016/j.resconrec.2017.10.036

Cai, M., Ren, C., Xu, Y., Lau, K. K.-L., & Wang, R. (2018). Investigating the relationship between local climate zone and land surface temperature using an improved WUDAPT methodology–A case study of Yangtze River Delta, China. *Urban Climate, 24*, 485-502.

Cai, M., Shi, Y., Ren, C., Yoshida, T., Yamagata, Y., Ding, C., & Zhou, N. (2021). The need for urban form data in spatial modeling of urban carbon emissions in China: A critical review. *Journal of Cleaner Production*, 128792.

Chen, H., Zhang, X., Wu, R., & Cai, T. (2020). Revisiting the environmental Kuznets curve for city-level CO2 emissions: based on corrected NPP-VIIRS nighttime light data in China. *Journal of Cleaner Production, 268*. doi:10.1016/j.jclepro.2020.121575

Chung, L. C. H., Xie, J., & Ren, C. (2021). Improved machine-learning mapping of local climate zones in metropolitan areas using composite Earth observation data in Google Earth Engine. *Building and Environment, 199*, 107879.

Cui, Y., Zhang, W., Wang, C., Streets, D. G., Xu, Y., Du, M., & Lin, J. (2019). Spatiotemporal dynamics of CO2 emissions from central heating supply in the North China Plain over 2012–2016 due to natural gas usage. *Applied Energy, 241*, 245-256.

Development, N., & Commission, R. (2012). Second National Communication on Climate Change of the People's Republic of China. In: National Development and Reform Commission Beijing.

Doll, C. H., Muller, J.-P., & Elvidge, C. D. (2000). Night-time imagery as a tool for global mapping of socioeconomic parameters and greenhouse gas emissions. *AMBIO: a Journal of the Human Environment, 29*(3), 157-162.

Elvidge, C. D., Baugh, K., Zhizhin, M., Hsu, F. C., & Ghosh, T. (2017). VIIRS night-time lights. *International Journal of Remote Sensing, 38*(21), 5860-5879.

Elvidge, C. D., Baugh, K. E., Kihn, E. A., Kroehl, H. W., Davis, E. R., & Davis, C. W. (1997). Relation between satellite observed visible-near infrared emissions, population, economic activity and electric power consumption. *International Journal of Remote Sensing, 18*(6), 1373-1379.

Elvidge, C. D., Baugh, K. E., Zhizhin, M., & Hsu, F.-C. (2013). Why VIIRS data are superior to DMSP for mapping nighttime lights. *Proceedings of the Asia-Pacific Advanced Network, 35*(0), 62. doi:10.7125/apan.35.7

Ghosh, T., Elvidge, C. D., Sutton, P. C., Baugh, K. E., Ziskin, D., & Tuttle, B. T. (2010). Creating a Global Grid of Distributed Fossil Fuel CO2 Emissions from Nighttime Satellite Imagery. *Energies, 3*(12), 1895-1913. doi:10.3390/en3121895

Gong, P., Chen, B., Li, X., Liu, H., Wang, J., Bai, Y., . . . Feng, S. (2020). Mapping essential urban land use categories in China (EULUC-China): Preliminary results for 2018. *Science Bulletin, 65*(3), 182-187.

Gurney, K. R., Mendoza, D. L., Zhou, Y., Fischer, M. L., Miller, C. C., Geethakumar, S., & de la Rue du Can, S. (2009). High resolution fossil fuel combustion CO2 emission fluxes for the United States. *Environ Sci Technol, 43*(14), 5535-5541.

Haines-Young, R., & Chopping, M. (1996). Quantifying landscape structure: a review of landscape indices and their application to forested landscapes. *Progress in physical geography, 20*(4), 418-445.

He, H. S., DeZonia, B. E., & Mladenoff, D. J. (2000). An aggregation index (AI) to quantify spatial patterns of landscapes. *Landscape Ecology, 15*(7), 591-601.

Hu, X., Belle, J. H., Meng, X., Wildani, A., Waller, L. A., Strickland, M. J., & Liu, Y. (2017). Estimating PM2. 5 concentrations in the conterminous United States using the random forest approach. *Environ Sci Technol, 51*(12), 6936-6944.

Huang, K., Xiao, Q., Meng, X., Geng, G., Wang, Y., Lyapustin, A., . . . Liu, Y. (2018). Predicting monthly high-resolution PM2. 5 concentrations with random forest model in the North China Plain. *Environmental Pollution, 242*, 675-683.

IEA. (2021). *World Energy Outlook 2021*. Retrieved from

IPCC. (2006). *2006 IPCC guidelines for national greenhouse gas inventories*: Intergovernmental Panel on Climate Change.

Khanna, N., Fridley, D., & Hong, L. (2014). China's pilot low-carbon city initiative: A comparative assessment of national goals and local plans. *Sustainable Cities and Society, 12*, 110-121.

Li, C., Song, Y., & Kaza, N. (2018). Urban form and household electricity consumption: A multilevel study. *Energy and Buildings, 158*, 181-193. doi:10.1016/j.enbuild.2017.10.007

Li, M., Liu, H., Geng, G., Hong, C., Liu, F., Song, Y., . . . Man, H. (2017). Anthropogenic emission inventories in China: a review. *National Science Review, 4*(6), 834-866.

Liu, Z., Guan, D., Wei, W., Davis, S. J., Ciais, P., Bai, J., . . . Marland, G. (2015). Reduced carbon emission estimates from fossil fuel combustion and cement production in China. *Nature, 524*(7565), 335-338.

Liu, Z., Ma, J., & Chai, Y. (2016). Neighborhood-scale urban form, travel behavior, and CO2 emissions in Beijing: implications for low-carbon urban planning. *Urban Geography, 38*(3), 381-400. doi:10.1080/02723638.2016.1191796

McGarigal, K., Cushman, S. A., & Ene, E. (2012). FRAGSTATS v4: spatial pattern analysis program for categorical and continuous maps. *Computer software program produced by the authors at the University of Massachusetts, Amherst. Available at the following web site: http://www. umass. edu/landeco/research/fragstats/fragstats. html*.

Meng, L., Graus, W., Worrell, E., & Huang, B. (2014). Estimating CO2 (carbon dioxide) emissions at urban scales by DMSP/OLS (Defense Meteorological Satellite Program's Operational Linescan System) nighttime light imagery: Methodological challenges and a case study for China. *Energy, 71*, 468-478. doi:10.1016/j.energy.2014.04.103

Mills, S., Weiss, S., & Liang, C. (2013). *VIIRS day/night band (DNB) stray light characterization and correction.* Paper presented at the Earth Observing Systems XVIII.

National Bureau of Statistics of China. (2016). *China Energy Statistical Yearbook [Chinese Document]*. Retrieved from Beijing, China:

National Development and Reform Commission of China. (2010). *The notice of piloting low-carbon provinces and low-carbon cities (2010)*. Retrieved from http://www.sdpc.gov.cn/zcfb/zcfbtz/2010tz/t20100810_365264.htm

Neel, M. C., McGarigal, K., & Cushman, S. A. (2004). Behavior of class-level landscape metrics across gradients of class aggregation and area. *Landscape Ecology, 19*(4), 435-455.

Ou, J., Liu, X., Li, X., Li, M., & Li, W. (2015). Evaluation of NPP-VIIRS Nighttime Light Data for Mapping Global Fossil Fuel Combustion CO2 Emissions: A Comparison with DMSP-OLS Nighttime Light Data. *PLoS One, 10*(9), e0138310. doi:10.1371/journal.pone.0138310

Ou, J., Liu, X., Li, X., & Shi, X. (2015). Mapping global fossil fuel combustion CO 2 emissions at high resolution by integrating nightlight, population density, and traffic network data. *IEEE Journal of Selected Topics in Applied Earth Observations and Remote Sensing, 9*(4), 1674-1684.

Pei, J., Niu, Z., Wang, L., Song, X.-P., Huang, N., Geng, J., . . . Jiang, H.-H. (2018). Spatial-temporal dynamics of carbon emissions and carbon sinks in economically developed areas of China: a case study of Guangdong Province. *Sci Rep, 8*(1), 1-15.

Penazzi, S., Accorsi, R., & Manzini, R. (2019). Planning low carbon urban-rural ecosystems: An integrated transport land-use model. *Journal of Cleaner Production, 235*, 96-111.

Ren, C., Ng, E., Mills, G., Ching, J., Bechel, B., See, L., . . . ALIAGA, D. G. (2017). *WUDAPT Global Initiative: Census of Global Cities* Retrieved from

Rong, P., Zhang, Y., Qin, Y., Liu, G., & Liu, R. (2020). Spatial patterns and driving factors of urban residential embedded carbon emissions: An empirical study in Kaifeng, China. *J Environ Manage, 271*. doi:10.1016/j.jenvman.2020.110895

Shan, Y., Guan, D., Liu, J., Mi, Z., Liu, Z., Liu, J., . . . Zhang, Q. (2017). Methodology and applications of city level CO 2 emission accounts in China. *Journal of Cleaner Production, 161*, 1215-1225. doi:10.1016/j.jclepro.2017.06.075

Shan, Y., Guan, Y., Hang, Y., Zheng, H., Li, Y., Guan, D., . . . Hubacek, K. (2022). City-level emission peak and drivers in China. *Science Bulletin*. doi:https://doi.org/10.1016/j.scib.2022.08.024

Shi, K., Chen, Y., Yu, B., Xu, T., Chen, Z., Liu, R., . . . Wu, J. (2016). Modeling spatiotemporal CO2 (carbon dioxide) emission dynamics in China from DMSP-OLS nighttime stable light data using panel data analysis. *Applied energy, 168*, 523-533. doi:10.1016/j.apenergy.2015.11.055

Shi, Y., Ren, C., Lau, K. K.-L., & Ng, E. (2019). Investigating the influence of urban land use and landscape pattern on PM2. 5 spatial variation using mobile monitoring and WUDAPT. *Landscape and Urban Planning, 189*, 15-26.

Small, C., Pozzi, F., & Elvidge, C. D. (2005). Spatial analysis of global urban extent from DMSP-OLS night lights. *Remote Sensing of Environment, 96*(3-4), 277-291.

State Council of China. (2019). *Strategy for integrated development of the Yangtze River Delta*. Retrieved from http://www.gov.cn/zhengce/2019-12/01/content_5457442.htm

Stewart, I. D., Oke, T. R., & Krayenhoff, E. S. (2014). Evaluation of the 'local climate zone'scheme using temperature observations and model simulations. *International journal of climatology, 34*(4), 1062-1080.

Tang, D., Zhang, Y., & Bethel, B. J. (2019). An analysis of disparities and driving factors of carbon emissions in the Yangtze River Economic Belt. *Sustainability, 11*(8), 2362.

The World Bank. (2020). CO2 emissions (metric tons per capita). Retrieved from https://data.worldbank.org/indicator/EN.ATM.CO2E.PC

Tibshirani, R. (1996). Regression shrinkage and selection via the lasso. *Journal of the Royal Statistical Society: Series B (Methodological), 58*(1), 267-288.

Tischendorf, L., & Fahrig, L. (2000). On the usage and measurement of landscape connectivity. *Oikos, 90*(1), 7-19.

Wang, J., Cai, B., Zhang, L., Cao, D., Liu, L., Zhou, Y., . . . Xue, W. (2014). High resolution carbon dioxide emission gridded data for China derived from point sources. *Environ Sci Technol, 48*(12), 7085-7093. doi:10.1021/es405369r

Wang, R., Cai, M., Ren, C., Bechtel, B., Xu, Y., & Ng, E. (2019). Detecting multi-temporal land cover change and land surface temperature in Pearl River Delta by adopting local climate zone. *Urban Climate, 28*, 100455.

Wang, W., Cao, C., Bai, Y., Blonski, S., & Schull, M. A. (2017). Assessment of the NOAA S-NPP VIIRS geolocation reprocessing improvements. *Remote Sensing, 9*(10), 974.

Wang, Y., Hayashi, Y., Chen, J., & Li, Q. (2014). Changing Urban Form and Transport CO2 Emissions: An Empirical Analysis of Beijing, China. *Sustainability, 6*(7), 4558-4579. doi:10.3390/su6074558

Xia, L., Zhang, Y., Sun, X., & Li, J. (2017). Analyzing the spatial pattern of carbon metabolism and its response to change of urban form. *Ecological Modelling, 355*, 105-115. doi:10.1016/j.ecolmodel.2017.03.002

Xinhua. (2020). Xi's statements at UN meetings demonstrate China's global vision, firm commitment. *Xinhuanet*. Retrieved from http://www.xinhuanet.com/english/2020-10/02/c_139414628.htm

Xu, Y., Ho, H. C., Wong, M. S., Deng, C., Shi, Y., Chan, T.-C., & Knudby, A. (2018). Evaluation of machine learning techniques with multiple remote sensing datasets in estimating monthly concentrations of ground-level PM2. 5. *Environmental Pollution, 242*, 1417-1426.

Yeh, A. G.-O., & Li, X. (2001). A constrained CA model for the simulation and planning of sustainable urban forms by using GIS. *Environment and Planning B: Planning and Design, 28*(5), 733-753.

Yu, X., Wu, Z., Zheng, H., Li, M., & Tan, T. (2020). How urban agglomeration improve the emission efficiency? A spatial econometric analysis of the Yangtze River Delta urban agglomeration in China. *J Environ Manage, 260*, 110061.

Yuan, C., Ng, E., & Norford, L. K. (2014). Improving air quality in high-density cities by understanding the relationship between air pollutant dispersion and urban morphologies. *Building and Environment, 71*, 245-258.

Zhang, Y., Pan, J., Zhang, Y., & Xu, J. (2021). Spatial-temporal characteristics and decoupling effects of China's carbon footprint based on multi-source data. *Journal of Geographical Sciences, 31*(3), 327-349. doi:10.1007/s11442-021-1839-7

Zhao, J., Chen, Y., Ji, G., & Wang, Z. (2018). Residential carbon dioxide emissions at the urban scale for county-level cities in China: A comparative study of nighttime light data. *Journal of Cleaner Production, 180*, 198-209. doi:10.1016/j.jclepro.2018.01.131

Zhao, J., Ji, G., Yue, Y., Lai, Z., Chen, Y., Yang, D., . . . Wang, Z. (2019). Spatio-temporal dynamics of urban residential CO2 emissions and their driving forces in China using the integrated two nighttime light datasets. *Applied Energy, 235*, 612-624.

Zhao, J., Zhang, S., Yang, K., Zhu, Y., & Ma, Y. (2020). Spatio-temporal variations of co2 emission from energy consumption in the yangtze river delta region of china and its relationship with nighttime land surface temperature. *Sustainability (Switzerland), 12*(20), 1-17. doi:10.3390/su12208388

Zhou, Y., Shan, Y., Liu, G., & Guan, D. (2018). Emissions and low-carbon development in Guangdong-Hong Kong-Macao Greater Bay Area cities and their surroundings. *Applied Energy, 228*, 1683-1692.

Fig 1

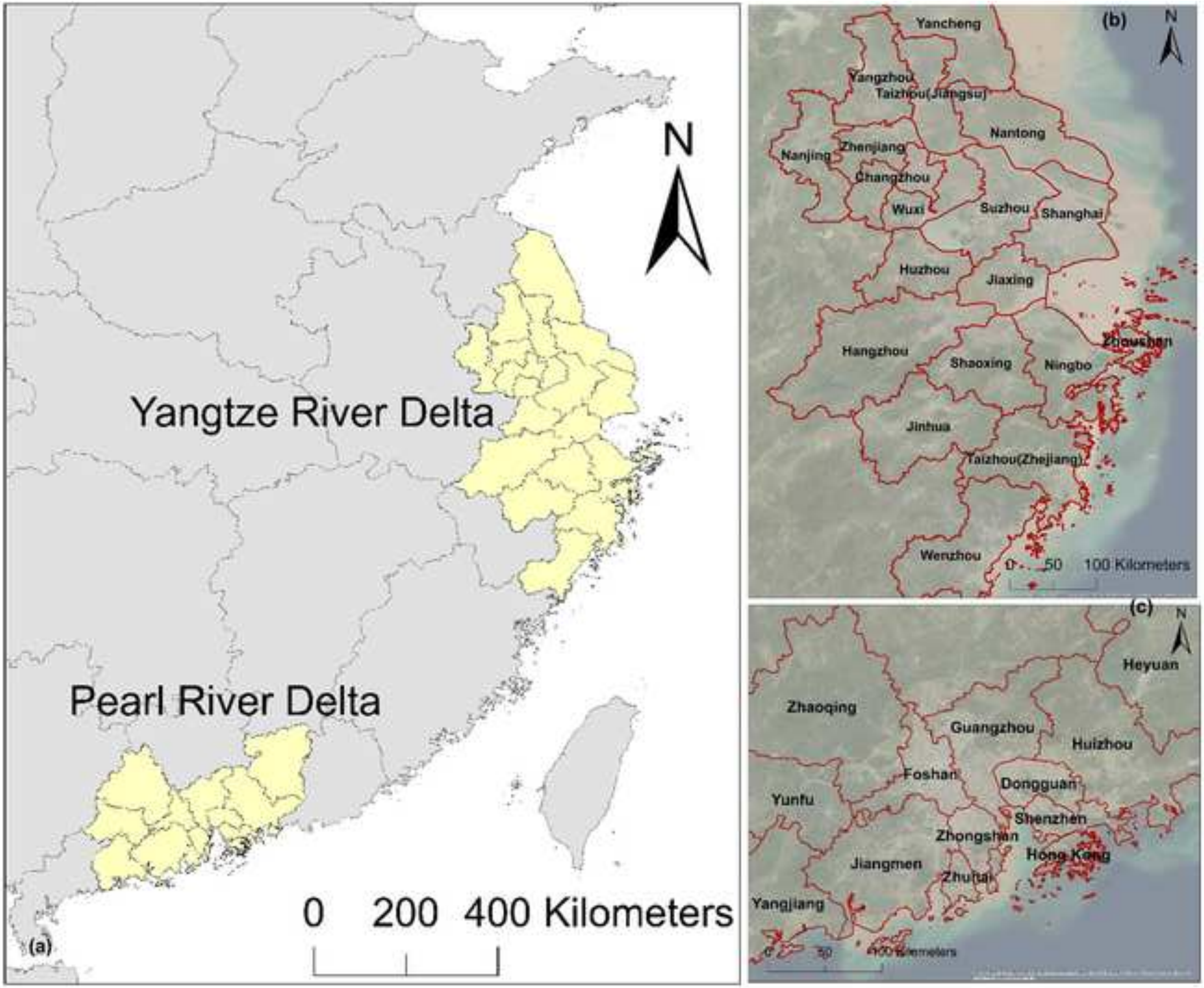

N
Yangtze River Delta
Pearl River Delta
0 200 400 Kilometers
(a)
(b)
Yancheng
Yangzhou
Taizhou(Jiangsu)
Nantong
Nanjing
Zhenjiang
Changzhou
Wuxi
Suzhou
Shanghai
Huzhou
Jiaxing
Hangzhou
Shaoxing
Ningbo
Zhoushan
Jinhua
Taizhou(Zhejiang)
Wenzhou
0 50 100 Kilometers
(c)
Heyuan
Zhaoqing
Guangzhou
Huizhou
Foshan
Dongguan
Yunfu
Shenzhen
Zhongshan
Hong Kong
Jiangmen
Zhuhai
Yangjiang
0 50 100 Kilometers

Fig 2

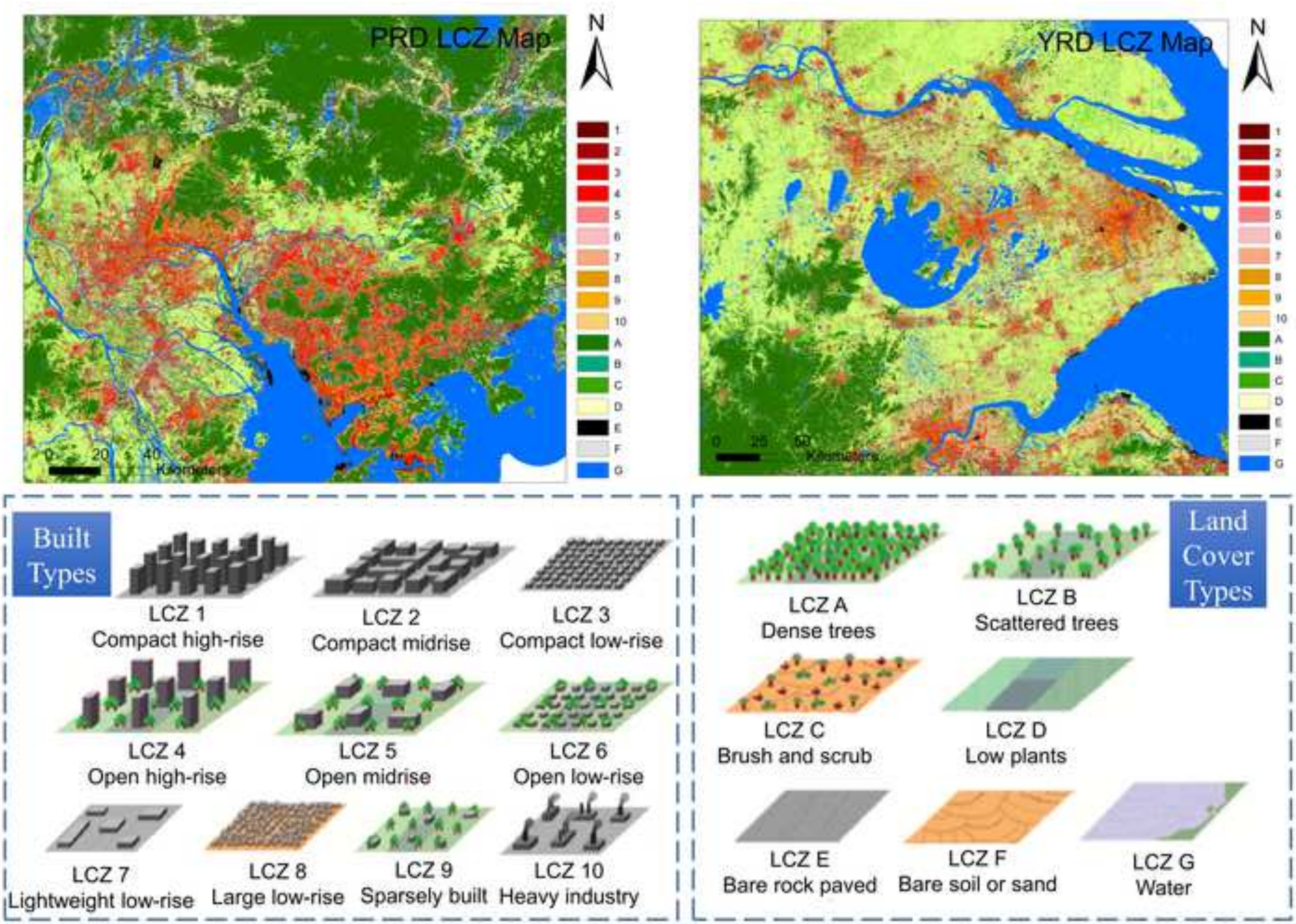
PRD LCZ Map
YRD LCZ Map
N
1
2
3
4
5
6
7
8
9
10
A
B
C
D
E
F
G
0 20 40
Kilometers
0 25 50
Kilometers
Built Types
LCZ 1
Compact high-rise
LCZ 2
Compact midrise
LCZ 3
Compact low-rise
LCZ 4
Open high-rise
LCZ 5
Open midrise
LCZ 6
Open low-rise
LCZ 7
Lightweight low-rise
LCZ 8
Large low-rise
LCZ 9
Sparsely built
LCZ 10
Heavy industry
Land Cover Types
LCZ A
Dense trees
LCZ B
Scattered trees
LCZ C
Brush and scrub
LCZ D
Low plants
LCZ E
Bare rock paved
LCZ F
Bare soil or sand
LCZ G
Water

Fig 3

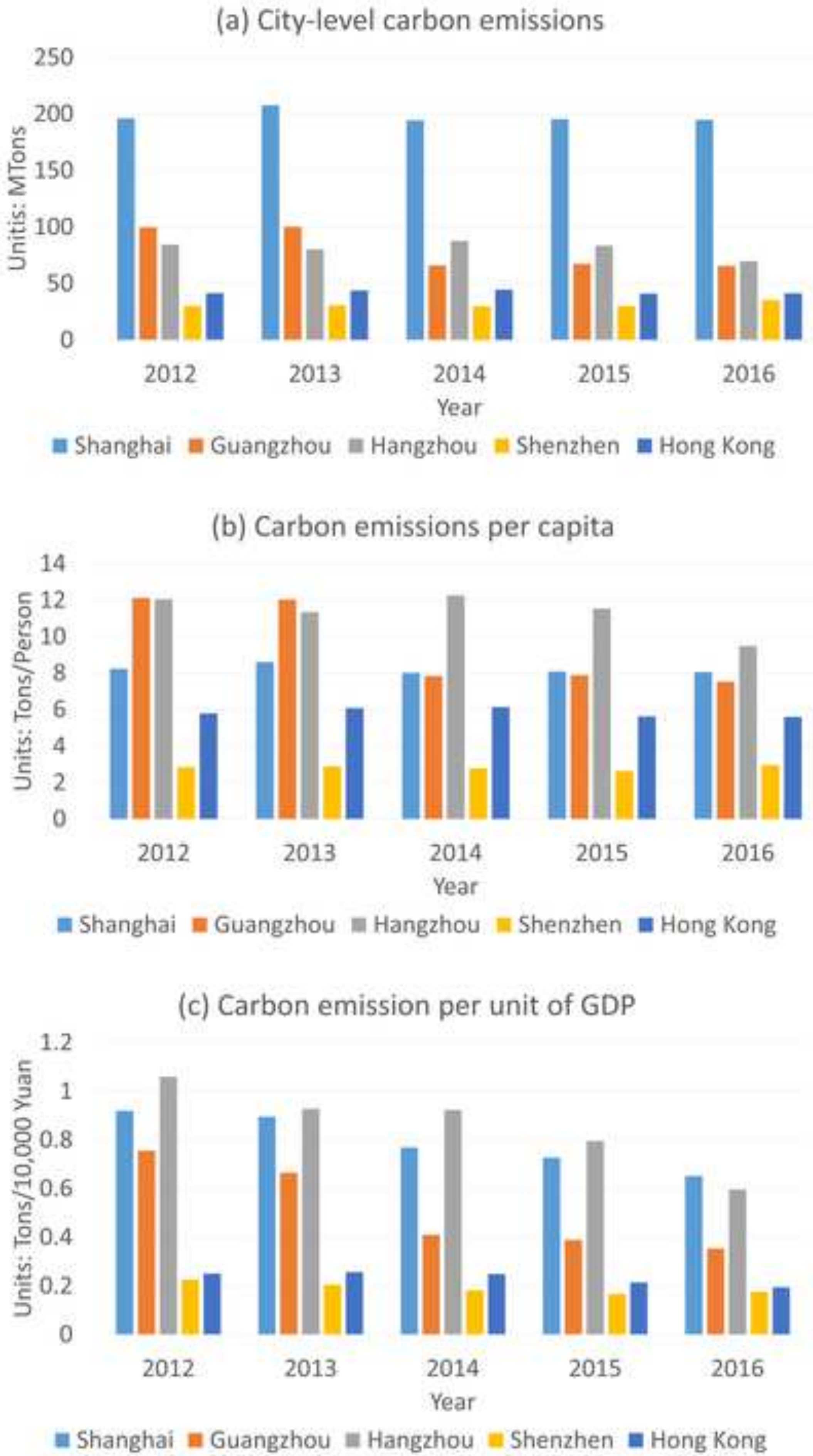
(a) City-level carbon emissions
Units: MTons
250
200
150
100
50
0
2012
2013
2014
2015
2016
Year
Shanghai
Guangzhou
Hangzhou
Shenzhen
Hong Kong
(b) Carbon emissions per capita
Units: Tons/Person
14
12
10
8
6
4
2
0
2012
2013
2014
2015
2016
Year
Shanghai
Guangzhou
Hangzhou
Shenzhen
Hong Kong
(c) Carbon emission per unit of GDP
Units: Tons/10,000 Yuan
1.2
1
0.8
0.6
0.4
0.2
0
2012
2013
2014
2015
2016
Year
Shanghai
Guangzhou
Hangzhou
Shenzhen
Hong Kong

Fig 4

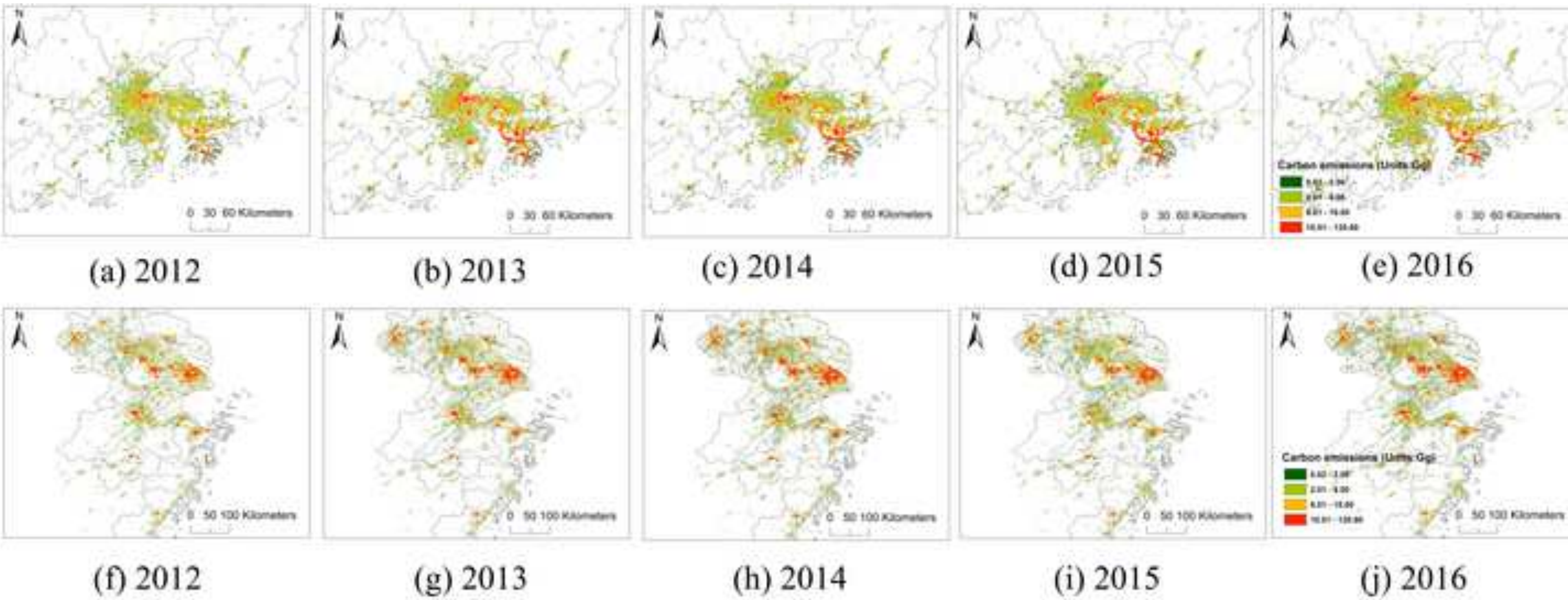
N
0 30 60 Kilometers
0 50 100 Kilometers
Carbon emissions (Units Gg)
(a) 2012
(b) 2013
(c) 2014
(d) 2015
(e) 2016
(f) 2012
(g) 2013
(h) 2014
(i) 2015
(j) 2016

Fig 5

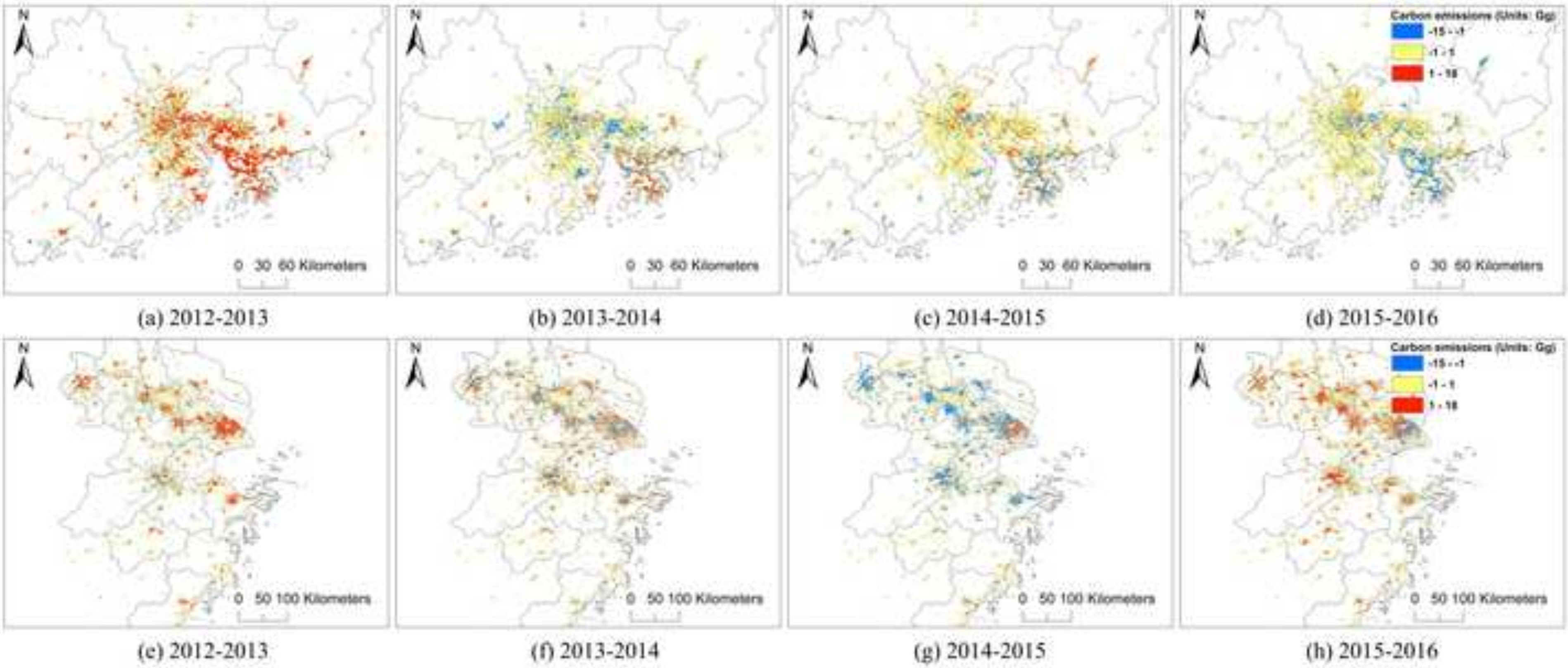
N
0 30 60 Kilometers
0 50 100 Kilometers
Carbon emissions (Units: Gg)
-15 - -1
-1 - 1
(a) 2012-2013
(b) 2013-2014
(c) 2014-2015
(d) 2015-2016
(e) 2012-2013
(f) 2013-2014
(g) 2014-2015
(h) 2015-2016

Fig 6

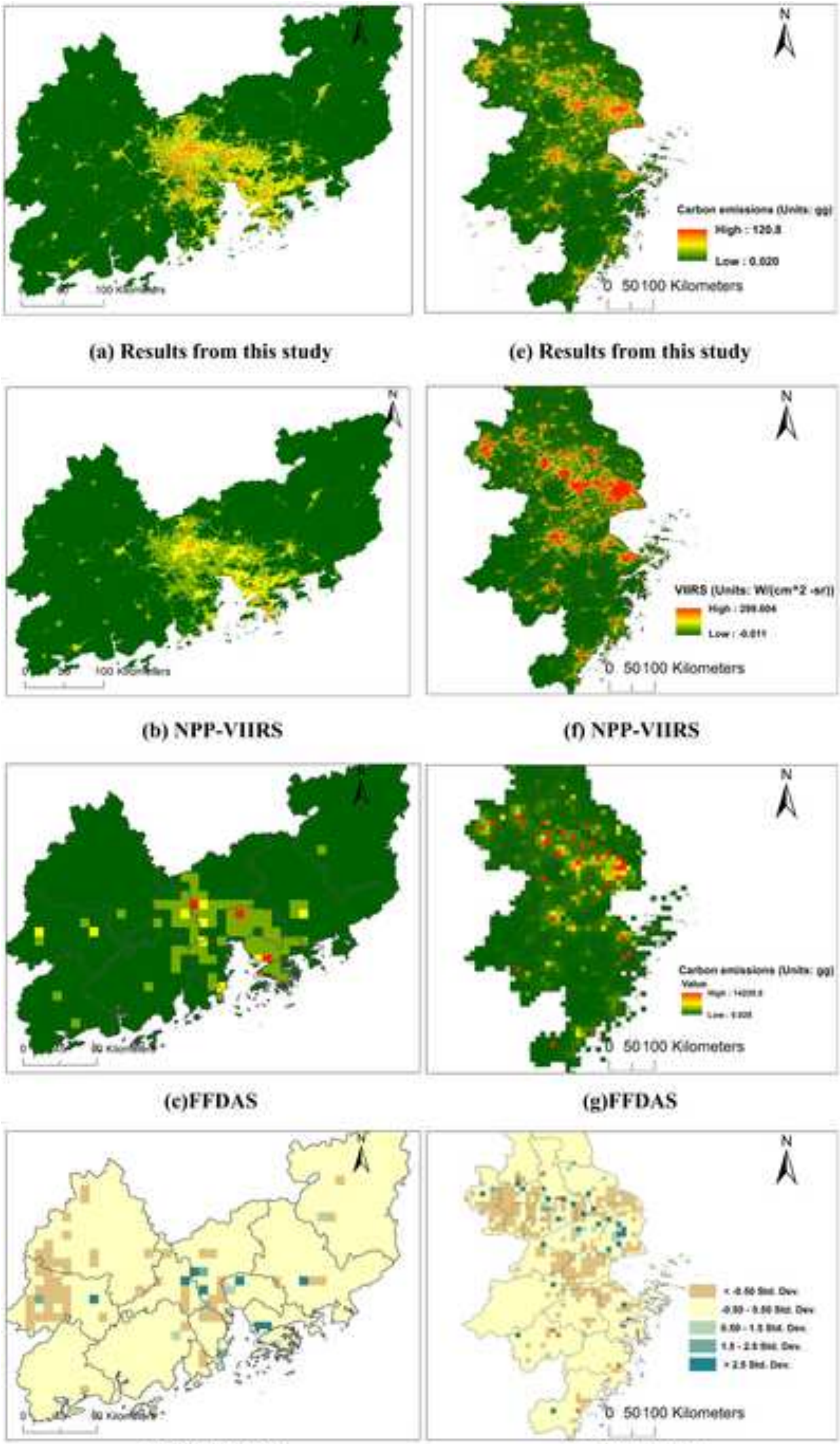

(a) Results from this study (e) Results from this study

(b) NPP-VIIRS (f) NPP-VIIRS

(c)FFDAS (g)FFDAS

(d)FFDAS-PRE (h) FFDAS-PRE